LoRadar: Enabling Concurrent Radar Sensing and LoRa Communication

Qianyi Huang, Zhiqing Luo, Jin Zhang, *Member, IEEE,* Wei Wang, *Member, IEEE,* Qian Zhang, *Fellow, IEEE*

Abstract—Miniature radar has demonstrated its great potential in smart homes, such as understanding the wellness of the residents and providing ubiquitous interactions. While it has many promising applications, it also results in congested RF (radio frequency) environments as there is an unprecedented amount of traffic in a smart home. To ease the strain on the limited spectrum, we ask the question that, can we reuse the sensing signals for data communication? With such a capability, we can improve the spectrum utilization by sharing the spectrum between sensing and communication systems. However, radar signals are customized for the sensing purpose and are incompatible with legacy communication standards. To address this challenge, we have an observation that, non-linearity effect in RF circuits can convert wideband radar signals into a LoRa signal. Based on this observation, in this paper, we present LoRadar, which enables an FMCW (Frequency-Modulated Continuous Wave) radar to carry LoRa signals in sensing waves. We present both the downlink and uplink design, enabling a LoRadar device to communicate with LoRa nodes in a bi-directional way. We implement LoRadar and evaluation results show that LoRadar can achieve home-level coverage with 3.4kbps data rate while it preserves the sensing resolution of the radar.

Index Terms—Radar sensing, LoRa communication, joint sensing and communication, non-linearity

1 Introduction

RADAR, traditionally thought of as bulky, expensive and limited to the military, now becomes a miniature device and are entering our homes with promising capabilities. Compared with vision-based approaches and on-body solutions, RF radar can operate in non-line-of-sight scenarios and is totally unobtrusive. Compared with Wi-Fi sensing, radar can achieve better sensing resolution, such as fine-grained human posture estimation [1]. Given these appealing properties, many research efforts have been devoted to exploring the great potential of radar sensing in smart homes, such as enabling ubiquitous gesture interaction [2], providing health-care services [3], [4] and tracking the 3D motion of the residents [5].

As the wireless spectrum is the shared medium, when the sensing device is transmitting radio waves from time to time, it results in congested RF environments. To make the situation worse, there is an unprecedented number of intelligent devices (e.g., smart speakers, smart HVAC systems, security and surveillance systems) in a smart home, which all require wireless resources for data communication and control message exchange. To ease the spectral congestion, we ask the question that, can we reuse the sensing signals for data communication? If it is possible, we can improve spectrum utilization and alleviate the uneasy coexistence between the sensing and communication systems.

However, here is the dilemma. Radar signals are wideband signals while home IoT devices are usually narrowband transceivers (*e.g.*, 1MHz for Bluetooth, 125kHz for LoRa). For an FMCW radar, it will continuously sweep a wide frequency band while an IoT device transmits/receives signals at a specific channel. The problem is how to embed a narrowband data signal into a wideband frequency sweeping signal. We observe that it is possible to create a narrowband signal by combining two wideband signals using RF non-linearity [6], [7]. Given two signals S_1(frequency f_1) and S_2(frequency f_2), non-linearity in RF circuits will create harmonics of incoming signals. Thus, in addition to the fundamental frequencyf_1 and f_2, there will be harmonics at frequency $2f_1$, $2f_2$, $f_1 + f_2$ and $f_1 - f_2$. While S_1 and S_2 could be frequency sweeping signals, their harmonics $f_1 - f_2$ could be a narrowband signal. It brings the feasibility that an IoT device can combine the sensing signals transmitted by two TX antennas on the radar and create a narrowband signal. In this way, we can enable the radar to sense the ambient environment while communicating with ubiquitous IoT devices in a smart home.

Although the idea sounds straight-forward, there are two major challenges. The first challenge is to design the dual-function radar signals, where the signals on both TX antennas should preserve the sensing accuracy while their joint harmonics can be decoded by an IoT device. The desired harmonic should be a signal that fully complies with the communication standard of the IoT devices. In other words, it should be a signal at the legitimate frequency with the right modulation scheme. We address this challenge in two steps. We first introduce a time offset between the sensing signals transmitted by the two TX antennas. When the two linear chirps sweep the same frequency band and

- *Q. Huang is with the Institute of Future Networks, Southern University of Science and Technology and Peng Cheng Laboratory, China.*
- *Z. Luo and W. Wang are with the School of Electronic Information and Communications, Huazhong University of Science and Technology, China.*
- *J. Zhang is with the Department of Computer Science and Engineering, Southern University of Science and Technology, China.*
- *Q. Zhang is with the Department of Computer Science and Engineering, Hong Kong University of Science and Technology, Hong Kong SAR, China.*

their time offset is half of the chirp duration, the desired harmonic (*i.e.*, $|f_1 - f_2|$) will become a constant wave, which can serve as the carrier wave for data signals. Then we embed modulated data symbols into the signal on one antenna, which will be coupled to the harmonic. In this way, the harmonic is a legitimate signal for the IoT device.

The second challenge is how to enable the radar to decode uplink transmission. The receiving chain in the FMCW radar is designed for the sensing task but not for data communication. To serve as both a sensing and communication device, the radar needs to collect targets' reflected signals and decode uplink transmission simultaneously. To address this challenge, we propose a new design for the receiving chain. To perform data decoding, we create a "local oscillator" for down-converting the data signals by mixing the radar signals on the TX chains. To prevent down-converted data signals and sensing signals from interfering with each other, we separate them at the baseband according to their frequency-domain characteristics.

To put it together, in this paper, we propose LoRadar, which enables an FMCW radar to communicate with a LoRa transceiver, as LoRa has shown growing popularity in smart home management [8]. A LoRadar device can communicate with LoRa nodes in a bidirectional way, while preserving radar's sensing capability and granularity. For downlink transmission, we design a simple, battery-free non-linear circuit using a Schottky diode, which is put between the antenna and the LoRa chipset. When the sensing signals transmitted by the radar resonate at the antenna, the non-linear circuit will generate a harmonic which turns out to be a standard LoRa signal. To enable uplink transmission, we redesign the receiving chain so that a LoRadar device can pick up the targets' reflections and decode LoRa packets simultaneously. Evaluation results show that LoRadar can achieve home-level coverage. It can work robustly in non-line-of-sight scenarios and at the presence of human activity. LoRadar can also decode orthogonal LoRa transmissions in the same frequency band. As for the sensing performance, the dual-function radar signals can preserve the sensing resolution of the FMCW radar.

We summarize our contributions as follows:

- We are the first to enable concurrent radar sensing and LoRa communication. It can improve spectrum utilization by sharing the spectrum between the sensing and communication systems in a smart home.
- We present LoRadar, a system that enables radar and LoRa nodes to communicate in a bi-directional way. We design dual-function radar signals for both sensing and LoRa communication, and propose a new design for the receiving chain.
- We implement LoRadar and evaluate its performance from various aspects. Evaluation results show that LoRadar can achieve home-level coverage and preserve the sensing resolution of radar.

2 Primer

2.1 Primer on FMCW Radar

FMCW is short for frequency-modulated continuous wave, where the frequency of the signal increases linearly with time, as shown in Figure 1. The working principle of an

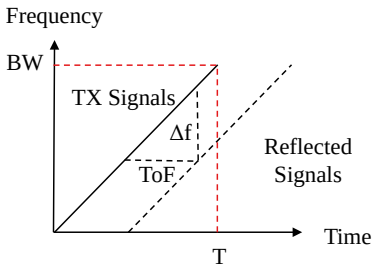

Fig. 1. The working principle of FMCW radar. A linear frequency modulated signal is transmitted from the radar. When it gets reflected by objects, the radar will compare the frequency offset between the transmitted and reflected wave to estimate the time-of-flight parameter.

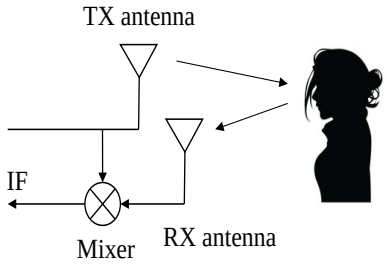

Fig. 2. The receiving chain in FMCW radar. The reflected signal is mixed with the transmitted signal. The mixer will output the IF signal whose frequency is Δf.

FMCW radar is as follows. The radar transmits a linear frequency-modulated wave and the wave will get bounced off from objects. Each reflection from an object is a delayed copy of the transmitted signals. FMCW radar transforms time-of-flight measurement (τ) into measuring the frequency offset (Δf) between the transmitted wave and the reflected wave, where τ and Δf preserve the following relationship,

$$\tau = \frac{\Delta f}{R},$$

where $R = \frac{BW}{T}$ is the ramp rate of the linear chirp. Figure 2 shows the receiving chain in an FMCW radar. The received signal is mixed with the transmitted signal. The output from the mixer is the IF signal, whose frequency is the difference of the two inputs, *i.e.*, Δf.

The ranging resolution depends on the radar's ability to distinguish two nearby locations, which depends on the frequency resolution of Δf. We calculate Δf by performing FFT on the baseband signal over a chirp duration T and thus, the frequency resolution is $f_{res} = \frac{1}{T}$. Transforming it into distance resolution, we have

$$d_{res} = \frac{1}{2}\tau_{res} \cdot c = \frac{1}{2} \cdot \frac{f_{res}}{R} \cdot c = \frac{1}{T \cdot 2R} \cdot c = \frac{c}{2BW}. \quad (1)$$

This brings the statement that ranging resolution is inversely proportional to the signal bandwidth. For two objects that are separated by a distance larger than d_{res}, their reflections will fall into different FFT bins and thus their movements can be decoupled. It indicates that FMCW radar can track multiple targets-of-interest simultaneously [5], [9].

In addition to Δf, another dimension that we could explore for sensing is the phase of the IF signal. The phase

of the IF signal is also related to the distance between the object and radar:

$$\phi = 2\pi \frac{2d}{\lambda}, \tag{2}$$

where λ is the wavelength of the signal. As phase is a value wrapped into $[0, 2\pi]$, it cannot tell the absolute distance but we can obtain the displacement of the target.

Combining the frequency and phase information, we can know the distance between targets to the radar and track each target's movement at a fine granularity.

2.2 Primer on LoRa

As the number of IoT devices increases dramatically, Low Power Wide Area Networks (LPWAN) are gaining increasing attention. LoRa, which promises long range communication and years of battery life, is becoming popular.

LoRa adopts chirp spread spectrum (CSS) modulation. CSS modulation has two key parameters, *i.e.*, the spreading factor SF and the bandwidth bw. In CSS modulation, the baseline chirp is a linear frequency modulated chirp from $-bw/2$ to $bw/2$, where the frequency increases linearly with time, shown as the Symbol 1 in Figure 3. The CSS modulation conveys information by cyclic time shifting the baseline chirp, where each cyclic shift represents a modulated symbol. Given a spreading factor of SF, there are total 2^{SF} possible cyclic shifts of the baseline chirp, *i.e.*, 2^{SF} different symbols. Thus, each symbol can represent SF bits of information. Figure 3 gives an example for the case where $SF = 2$. By tuning the combination of bandwidth and spreading factor, we can get different LoRa data rates, from tens of bps to tens of kbps. Currently, LoRa supports seven spreading factors, from SF7 to SF12. Possible bandwidths range from 7.8kHz to 500kHz. As a characteristic of CSS modulation, the LoRa receiver can demodulate simultaneous transmission of different SFs in the same channel, which supports the coexistence of multiple devices.

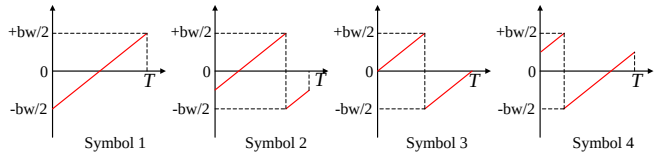

Fig. 3. LoRa symbols with CSS modulation. In this example, the spread factor SF is 2. There are $2^2 = 4$ possible cyclic shift of the baseline chirp and thus a symbol can represent 2 bits.

LoRa operates in unlicensed sub-GHz frequency bands, such as 433MHz, 868MHz and 915MHz, which is region specific.

3 Non-linearity for LoRadar

The key problem in LoRadar is to design dual-function signal waveforms that can serve as sensing signals and data signals simultaneously. Our insight is to exploit the non-linearity effect to bridge the frequency gap between wideband sensing signals and IoT data signals. In this section, we first introduce the non-linearity phenomenon in RF communication and then discuss how LoRadar can take advantage of this phenomenon to achieve joint radar-communication paradigm. Finally, we give an overview of LoRadar.

3.1 Non-linearity in RF Communication

RF circuits are supposed to be linear, that is, the output signal is a linear function of the input signal, *i.e.*,

$$S_{out} = \lambda S_{in}.$$

When the input signal is at frequency f, the output signal is also of frequency f. When the hardware is imperfect, a circuit will exhibit non-linear behaviour. The output signal becomes a non-linear function of the input signal, *i.e.*,

$$S_{out} = \lambda_1 S_{in} + \lambda_2 S_{in}^2 + \cdots. \tag{3}$$

When the input signal contains frequency f_1 and f_2, the output signal will contain not only the original frequencies f_1 and f_2, but also harmonics resulted from the non-linearity behaviour. Specifically, assume that the input signals are two sine waves, the second-order harmonics become

$$\begin{aligned}
&\lambda_2 S_{in}^2 = \lambda_2 \left[\sin(2\pi f_1 t) + \sin(2\pi f_2 t)\right]^2 \\
&= \lambda_2 \left[\sin^2(2\pi f_1 t) + \sin^2(2\pi f_2 t) + 2\sin(2\pi f_1 t)\sin(2\pi f_2 t)\right] \\
&= \frac{\lambda_2}{2}\left[2 - \cos(2\pi 2 f_1 t) - \cos(2\pi 2 f_2 t) + 2\cos(2\pi(f_1 - f_2)t)\right. \\
&\left. -2\cos(2\pi(f_1 + f_2)t)\right].
\end{aligned}$$

The output signal contains frequency $2f_1$, $2f_2$, $f_1 - f_2$ and $f_1 + f_2$. These harmonics are considered distortion of the original signal and RF circuits are usually designed to avoid such non-linearity phenomenon.

Among the second-order harmonics, we are particularly interested in the term $f_1 - f_2$. When the two signals enter a non-linear circuit, there will be a harmonic whose frequency is the difference of the two input signals. Consider the case that the two input signals are both linear FMCW chirp sequences, as shown in Figure 4. The two chirps can be sensing signals transmitted by different antennas on a RF radar, as a RF radar usually have multiple TX-RX antenna pairs to handle multi-path reflections [5], [10]. The first chirp starts from f_1 and its frequency increases linearly with time at a ramp rate R; the second chirp starts at f_2 and also increases with time at the same rate. As their frequency difference is constant, the second-order harmonics will contain a component, which is a constant wave at frequency $f_2 - f_1$.

It brings the feasibility that we can exploit this non-linearity phenomenon to convert two wideband sensing signals into a narrowband data signal. This property of non-linearity enables the design for LoRadar.

3.2 Non-linear Circuit for LoRadar

Although there are non-linear components (*e.g.*, amplifiers) on commercial devices, their non-linear capabilities are device-specific. In order to guarantee the communication performance, LoRadar proposes a simple non-linear circuit, as shown in Figure 5.

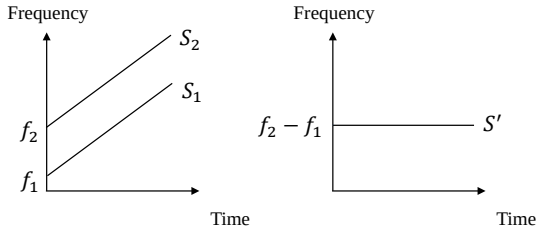

Fig. 4. The opportunity from non-linearity. The left figure shows two linear FMCW chirp sequences, the frequencies of which are both linearly increasing with time. As long as their frequency difference is a constant value, their second-order harmonics will contain a component which is a constant wave at frequency $f_2 - f_1$.

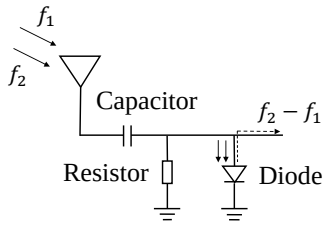

Fig. 5. The non-linear circuit. We use a schottky diode as the non-linear component. This diode will generate harmonics of the signals arriving at the antenna.

On the circuit, we use a Schottky diode [11] as the non-linear component. According to [12], the current-voltage characteristic of the diode is as follows:

$$I = I_s \left(e^{\frac{V_i}{V_T}} - 1 \right) + C \frac{\mathrm{d}V_i}{\mathrm{d}t},$$

where I_s is the saturation current of the diode, V_i is the voltage of the incoming signals, V_T is the thermal voltage and C is the junction capacitance. The diode is a non-linear device as the current of the diode is not linearly related to its terminal voltage. Expanding the exponential term using Fourier series brings the high-order harmonics [12].

This non-linear circuit is battery-free and can be put between the antenna and the transceiver. When the incoming signals from the antenna, containing frequency f_1 and f_2, pass through the diode, in addition to the fundamental frequencies, the output will contain the high-order harmonics at frequency $2f_1$, $2f_2$, $f_1 + f_2$, $f_2 - f_1$, *etc*. Due to the front-end filter at the receiver, out-of-band harmonics will be filtered out and only the in-band signal will enter the receiving chain. We can tune f_1 and f_2 so that the desired harmonic $f_2 - f_1$ is an in-band signal.

To demonstrate the performance of this circuit, we conduct a set of experiments. We use two USRP N210s with XCVR2450 daughter boards to generate two single-tone waves at f_1 and f_2. We connect the non-linear circuit to a Rohde & Schwarz FSH6 Handheld Spectrum Analyzer (100kHz-6GHz) and compare the received signal strength of the original frequency and the harmonic. For each combination of f_1 and f_2, we measure the signal strength at three different locations. The results are shown in Table 1. We can see that, when f_1 and f_2 is either 50MHz or $2.6G$Hz apart, the desired harmonic $f_2 - f_1$ exists in both cases.

	$f_1 = 2.4$ GHz	$f_2 = 2.45$ GHz	$f_2 - f_1$
L1 (1m)	-60.4 dBm	-35.5 dBm	-93.4 dBm
L2 (3m)	-66.5 dBm	-45.6 dBm	-112.7 dBm
L3 (5m)	-72.3 dBm	-54.8 dBm	-110.0 dBm
	$f_1 = 2.4$ GHz	$f_2 = 5$ GHz	$f_2 - f_1$
L1 (1m)	-52.4 dBm	-48.7 dBm	-99.1 dBm
L2 (3m)	-68.0 dBm	-49.2 dBm	-104.9 dBm
L3 (5m)	-72.3 dBm	-54.0 dBm	-113.0 dBm

TABLE 1
Performance of Non-linear Circuit. We use two USRPs to generate constant wave at f_1 and f_2 and measure the signal strength of the original signals and the harmonic at three locations.

In the top section of Table 1, when the receiver is 1m away from the transmitter, the received signal strength is -60.4 dBm at 2.4GHz, while in the bottom section, the number is -52.4 dBm. When the TX and RX is very close, the received signal strength is susceptible to subtle position differences. The 8dB differences are possibly due to the slight position/orientation differences. When the TX and RX are not in close proximity, as in the case of L2 and L3, the measurement results are very close.

As we can see from Section 3.1, the harmonic is the product of the two original signals. Thus, the amplitude of the harmonic is also the product of the two original signals' amplitudes. If the signal strength of the two original signals are both -40dBm, the power of the harmonic is -80dBm. The harmonic is much weaker than the original signal which requires that the receiver has good sensitivity.

Among various COTS devices, LoRa has good sensitivity down to -148 dBm. As stated by Semtech, smart homes and buildings are important application scenarios of LoRa technology, where LoRa can be used to connect low-power, low-rate sensors and actuators, such as smoke detector/humidity sensor, which do not require high data rate but long operation life. Thus, in this work, we target at enabling the radar to communicate with LoRa nodes. It is our future work to extend to other IoT devices, such as Bluetooth and Zigbee devices.

In order for the harmonic to be above -148dBm, the received signals should be no lower than -74dBm (we assume that the two signals are of similar power). Thus, we expect that the communication range is shorter than the standard LoRa.

3.3 LoRadar Overview

In this paper, we propose LoRadar, which can perform fine-grained sensing and bi-directional communication with LoRa nodes simultaneously. As shown in Figure 6, the LoRadar device is continuously performing sensing tasks. Meanwhile, it also serves as the LoRa gateway. When there is data for downlink transmission, *i.e.*, from the LoRadar device to a LoRa node, LoRadar will use the dual-function radar signals, which contain the LoRa packets. For the remaining time, LoRadar will use the original linear chirp signal and listen for uplink transmission. We summarize the high-level operations of LoRadar as follows.

Sensing. Similar to other RF radars, LoRadar accomplishes the sensing task by transmitting wideband sensing signals. These signals propagate in the air and get reflected by obstacles. By analyzing the reflections, LoRadar can

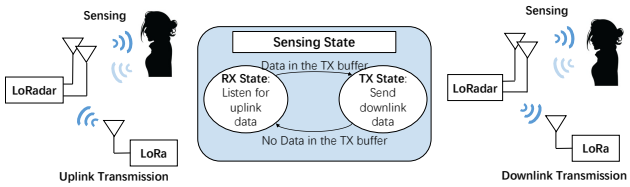

Fig. 6. LoRadar overview. The LoRadar is continuously performing sensing task. Meanwhile, it also serves as the LoRa gateway. When there is data in the TX buffer, LoRadar will perform downlink transmission. Otherwise, it will be in the RX state waiting for uplink transmission from LoRa nodes.

detect the presence and movement of objects and human bodies in the space.

Communication. Communication tasks are accomplished at the same time with the sensing tasks. For the downlink part, the sensing signals transmitted by the LoRadar device will resonate at the antenna on a LoRa node. The signals will enter the non-linear circuit and create a narrowband harmonic, which turns out to be a LoRa packet and can be decoded by the LoRa device. For the uplink part, the receiving chain in LoRadar is able to pick up both reflected sensing signals and uplink LoRa transmissions simultaneously. LoRadar separates these two types of signals apart and carry out corresponding processing individually.

As the working principle of the sensing functionality is very much the same as a normal FMCW radar, the following sections will focus on the communication part, describing the downlink and uplink design in LoRadar.

4 LoRadar Downlink Design

In this section, we describe the downlink design in LoRadar. We first present the design of the dual-function radar signals and then discuss the sensing performance of such signals.

4.1 Downlink Waveform Design

The key challenge in downlink design is to embed LoRa packets into FMCW signals while preserving the sensing capability. To create a LoRa signal from two FMCW waves, we need to create both the carrier frequency at the LoRa band and the CSS-modulated signals. In the following part, we first present how LoRadar creates the LoRa carrier frequency using two FMCW signals and then describe how to embed CSS-modulated signals into the sensing signals.

4.1.1 Create LoRa Carrier Wave

By non-linearity, we can convert two wideband signals into a narrowband signal. Let f_L denote the LoRa band, which could be 433MHz, 915MHz or other frequency bands that LoRa device can operate at. Let $f_1(t)$ and $f_2(t)$ be the frequency of signals transmitted by the two antennas on a LoRadar device. Assume that $f_1(t)$ and $f_2(t)$ both fall within $[f_a, f_b]$, the frequency band allocated for sensing, where $f_b - f_a = BW$. In order for the second harmonic to generate a tone at f_L, it needs to satisfy

$$f_L = |f_1(t) - f_2(t)|, \forall t \in [0, T], \tag{4}$$

where T is the chirp duration.

A simple solution is to guarantee that there is a constant frequency offset, *i.e.*, f_L, between the two signals. We can have f_1 sweep from f_a to $f_b - f_L$ while f_2 sweeps from $f_a + f_L$ to f_b. Although it could generate a carrier wave at f_L, in this way, the bandwidth of both signals is reduced by f_L. According to Equation (1), for FMCW radar, its sensing resolution is subject to the bandwidth of the signal. This will lead to lower sensing resolution, which is undesirable. In order to preserve the sensing accuracy, both signals should sweep the full band.

To achieve this goal, we come up with the following way to control the frequency sweep. The chirp on the first antenna is advanced by half of the chirp duration, as shown in Figure 7. Mathematically, it can be written as follows:

$$f_1(t) = \begin{cases} R \cdot t + \frac{BW}{2} & t < \frac{T}{2} \\ R \cdot t - \frac{BW}{2} & t \geq \frac{T}{2} \end{cases}, \qquad f_2(t) = R \cdot t, \tag{5}$$

where R is the slope of the FMCW chirp. When $BW = 2f_L$, in the first half of the chirp, we have $f_L = f_1(t) - f_2(t)$, while in the second half of the chirp, $f_L = f_2(t) - f_1(t)$. Thus, Equation (4) is satisfied.

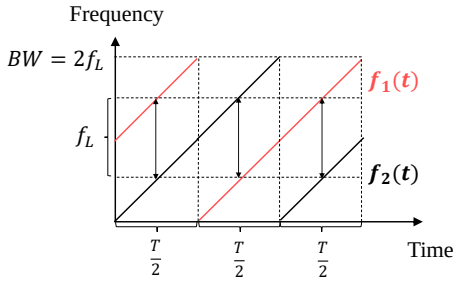

Fig. 7. Two unsynchronized FMCW chirps, with half chirp time offset. In this way, the two chirps can create a harmonic at frequency $\frac{BW}{2}$, while both chirps sweep the full sensing band. When $f_L = BW/2$, the harmonic can serve as the carrier wave for LoRa signals.

To verify this idea, we perform a feasibility study. We use a Keysight M8190A two-channel arbitrary waveform generator to generate two FMCW chirps according to Figure 7, where BW = 866MHz, T = 1ms and the center frequency is 900MHz. The chirp signals are amplified and transmitted. Figure 8(a) shows the spectrum of the chirp signals, measured by Rigol DSA 1030 spectrum analyzer. We connect a receiving antenna and the non-linear circuit to the RF input port of the spectrum analyzer. From Figure 8, we can see that, as expected, the non-linearity circuit creates a harmonic at $\frac{BW}{2}$ = 433MHz.

It proves that we can create a carrier wave at the desired frequency using this method, while both chirps sweep the whole bandwidth, without degrading the sensing accuracy.

4.1.2 Create CSS-Modulated Signals

LoRa signals, as shown in Figure 3, are linear chirps within the channel bandwidth. We use $S_L(t)$ to denote the frequency of LoRa signals as a function of time.

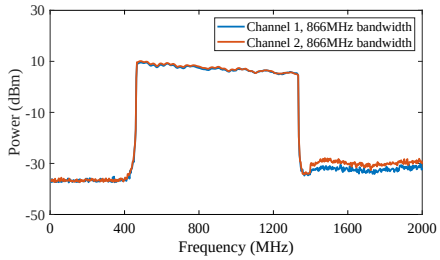

(a) Two linear chirps with 866MHz bandwidth.

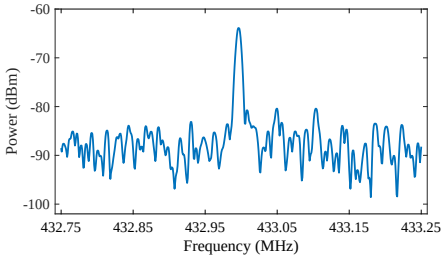

(b) Second-order harmonic at 433MHz

Fig. 8. Feasibility study. Two linear chirps are sweeping 866MHz band, with one chirp advanced by half chirp duration. We can get a desired harmonic at 433MHz.

As we discuss previously, in the first half of the FMCW chirp, the desired harmonic is created by $f_1(t) - f_2(t)$ while in the second half, the desired harmonic is created by $f_2(t) - f_1(t)$. Thus, to embed CSS-modulated signals into the sensing chirp, we also need to distinguish these two cases. In the first half of the chirp, $S_L(t)$ is added to $f_1(t)$, while in the second half, $-S_L(t)$ is added to $f_1(t)$. Finally, the sensing signal on the first antenna becomes

$$f_1^S(t) = \begin{cases} R \cdot t + f_L + S_L(t) & t < \frac{T}{2} \\ R \cdot t - f_L - S_L(t) & t \geq \frac{T}{2} \end{cases}. \quad (6)$$

In this way, the desired harmonic becomes

$$\left| f_1^S(t) - f_2(t) \right| = f_L + S_L(t),$$

where the right hand side is the LoRa signal at frequency f_L.

By creating the carrier wave and CSS-modulated signals separately, we can decouple the parameters for sensing signals and data signals. The FMCW chirp can select appropriate parameters (*e.g.*, chirp duration) according to the application scenarios while LoRa node can set its spreading factor and bandwidth according to the throughput demand. Next, we discuss its impact on the sensing performance.

4.2 Impact on Sensing Capability

LoRadar modifies the original sensing signal by embedding a narrowband CSS-modulated signal to the original FMCW chirp. This changes the original linear chirp in two aspects, as we show in Figure 9. The modified chirp presents slope discontinuity and frequency discontinuity. We analyze their impact on estimating frequency offset (Δf) individually.

Slope Discontinuity. The slope of the modified sensing chirp in the first and second half is different. Let R and r denote the slope of the FMCW sensing chirp and LoRa data

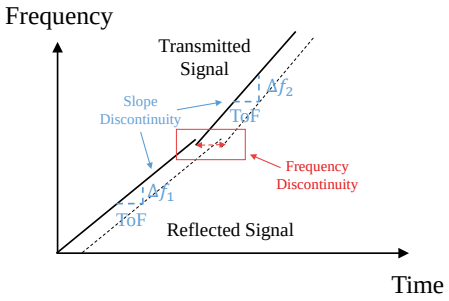

Fig. 9. Modified sensing signals. As we embed CSS-modulated signals into the original FMCW chirp, the modified signals present slop discontinuity and frequency discontinuity. We plot these discontinuities exaggeratively so that they become visible.

chirp respectively. The slope of the first half ($f \in [0, \frac{BW}{2}]$) is $R - r$ while the slope of the second half ($f \in [\frac{BW}{2}, BW]$) is $R + r$. Assume that the time-of-flight is τ, for the first half, $\Delta f_1 = (R - r)\tau$, while for the second half, $\Delta f_2 = (R + r)\tau$. As the FMCW chirp usually sweeps GHz bandwidth in milliseconds [3], [10], [13] while the LoRa data chirp just sweeps several hundreds of kHz (channel bandwidth, 500kHz at maximum). r is several orders of magnitude smaller than R and its impact on Δf_1 and Δf_2 is negligible. Thus, $\Delta f_1 \approx \Delta f_2 \approx R \cdot \tau$.

Frequency Discontinuity. The frequency of modified sensing chirp is not linearly increasing due to the frequency discontinuity in LoRa signal, either at the boundary of symbols or shift from $bw/2$ to $-bw/2$ within a symbol, as shown in Figure 3. The modified sensing signal becomes a piecewise function where each piece is a linear function. According to the working principle of FMCW radar, it determines the distance to the target by the frequency offset between the transmitted signals and the reflected signal, as the frequency offset is linearly proportional to the time-of-flight. Similarly, LoRadar can compare such a frequency-discontinuous signal with its delayed version. The result is that, for the majority of time, the frequency offset preserves the linear relationship with time-of-flight while for an extremely short window, which is highlighted in Figure 9, the linear relationship no longer holds due to the frequency discontinuity. The duration of this window is equal to the time-of-flight τ, which is at the level of nanoseconds. Compared to the whole chirp duration, usually at the level of milliseconds, this short window has almost no impact when we estimate the frequency offset using the signals of a complete chirp duration.

It is more straight-forward to analyze its impact on estimating phase. Whatever the waveform, the relationship between phase and distance (Equation (2)) preserves. Thus, modifying the sensing signals will not affect phase estimation.

Above is our analysis on the capability of the dual-function signal. We demonstrate in the Section 7 that it preserves the sensing resolution of FMCW radar.

5 LoRadar Uplink Design

In this section, we describe the uplink design in LoRadar.

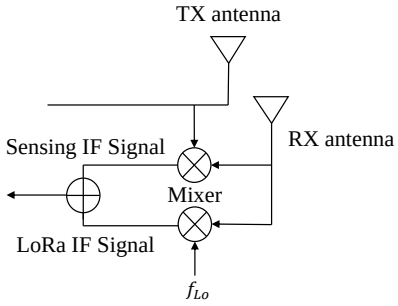

Fig. 10. The receiving chain in LoRadar. We create a "local oscillator" f_{LO} for uplink LoRa signals. We tune f_{LO} so that intermediate frequency of sensing and LoRa signals are separate in the frequency domain.

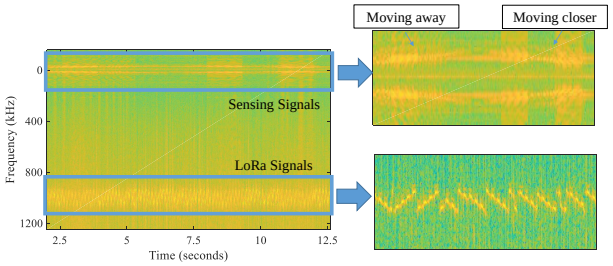

Fig. 11. A spectrogram of the received signal. The sensing IF signals fall at the low frequency part while LoRa signals are down-converted to 1MHz. In this way, we prevent the two types of signals from interfering with each other.

The receiver chain in FMCW radar is very different from a normal transceiver. As shown in Figure 2, the reflected signal is mixed with the transmitted signal, resulting in a low-frequency IF (intermediate frequency) signal, usually tens/hundreds of kilohertz. Thus, even though the signals transmitted by a radar is a wideband signal, it does not require a wideband receiver. Different from a normal RF radar, the LoRadar device needs to receive both the reflected sensing signals and the uplink LoRa transmissions in one shot.

To achieve this goal, there are two major challenges. First, uplink LoRa signals are centred at frequency f_L. When the received LoRa signals pass through the receiving chain, mixing with a wideband sweeping signal, the mixed signals will also become a wideband signal which cannot be captured by the receiver. Second, as we need to perform sensing and communication tasks simultaneously, we need to prevent these two types of signals from interfering with each other.

To address the first challenge, LoRadar creates a "local oscillator" for LoRa signals without using any additional hardware oscillator. LoRadar creates f_{LO} by mixing the signals on the two TX chains. According to Section 4, the two chirps are time offset by half the chirp duration. When doing uplink transmission, the signals on the TX chain are the original linear chirps without embedding the CSS-modulated signals. Mixing these two chirps creates a carrier wave at f_{LO}, where $f_{LO} = \frac{1}{2}BW$. It can serve as the local oscillator for decoding the LoRa signal. When S_L is mixed with this carrier wave, it is shifted to the intermediate frequency at $f_L - f_{LO}$.

To address the second challenge, we observe that the maximum value of Δf is known. Δf depends on the distance to the object and the slope of the chirp signal. Under a typical setting of the radar (*i.e.*, BW is several GHz, T at the millisecond level, 20m maximum detectable range in an indoor scenario), Δf usually falls between DC to 1MHz. In order to prevent sensing signals and data signals from interfering with each other, we can tune the frequency of f_{LO} so that sensing and LoRa signals are separate in the frequency domain at the baseband. We can select an appropriate f_{LO} such that $f_L - f_{LO}$ falls above Δf_{max}.

The receiving chain in LoRadar is shown in Figure 10. f_{LO} is created by mixing the chirps on the two TX chains, a linear chirp and its delayed version. According to Section 4, $f_{LO} = \frac{1}{2}BW$. To achieve the frequency guard, we set the uplink bandwidth BW_U to be

$$BW_U = 2f_{LO} = 2(f_L - \Delta f_{max}).$$

The RX chain in LoRadar has two paths. One path is the same as the original RX chain in a normal radar, where the received signal is mixed with the original chirp to obtain Δf. On the other path, the received signal is mixed with f_{LO}, shifting LoRa signals to the baseband. The resulted sensing IF signals and LoRa IF signals are both baseband signals and are separate in the frequency domain, so they can be captured by a baseband processor simultaneously.

Figure 11 gives the spectrogram of a 10s-segment signal. The LoRa node is transmitting uplink packets at $f_L = 433$MHz and we set BW_U to be 864MHz, *i.e.*, $f_{LO} = 432$MHz. Meanwhile, we move a laptop back and forth before the radar. We can see that the sensing IF signals fall at the low frequency part. The intermediate frequency first increases as we move the laptop away and then decreases as we bring the laptop closer. The LoRa IF signals are at 1MHz, as $f_L - f_{LO} = 1$MHz. Figure 11 indicates that we can prevent the two types of signals from interfering with each other.

An important feature in LoRa is that LoRa signals with different spreading factor are orthogonal to each other. Thus, there could be multiple LoRa devices, employing different spread factors, transmitting simultaneously in the same channel. As LoRadar preserves the property of LoRa signals, it supports concurrent LoRa transmission in the same channel. We verify this in Section 7.

6 Implementation

In this section, we describe the implementation details of LoRadar.

Transmitting chain of LoRadar. We use a KeySight M8190A arbitrary waveform generator to generate the sensing signals. M8190A supports dual-channel operation while each channel supports up to 2.4GHz sampling rate. Signals are generated via the SystemVue software running on a Windows 10 desktop and downloaded to the signal generator. The chirp signal is generated using the LFM module in SystemVue, where we can specify the center frequency, sweeping bandwidth and chirp duration. The time offset

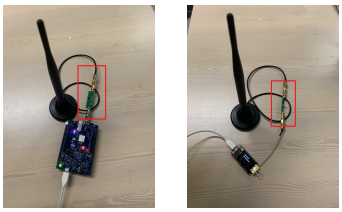

(a) SX1276. (b) SX1278.

Fig. 12. LoRa receiver with non-linear circuit (highlighted in rectangular).

between two TX chains is achieved by cyclic time shifting the chirp samples, where we move the second half of chirp samples before the first half.

We use a Matlab script to generate the CSS modulated signal. The signal is multiplied with the linear chirp from the LFM module, as time domain multiplication of two chirp signals results in a new chirp whose frequency is the summation of the original two chirps. We set the transmission power to be 8 dBm.

To demonstrate the feasibility of LoRadar on a software defined radio, we also implement the TX chains using NI USRP-2953R, which also supports dual-channel operation, each with 120MHz bandwidth. More details about this setup can be found in Section 7.1.6.

Receiving chain of LoRadar. We implement the receiving chain of LoRadar according to the schematic in Figure 10. Compared with the receiving chain in a FMCW radar, it has several extra components: a power splitter divides the received signal into two paths; a mixer takes the signals on the two TX chains and its output is connected to the LO port of a second mixer, where the second mixer down-converts the LoRa signals to the baseband; a power combiner combines the baseband signals from two paths and its output is fed into the LFRX-LF daughterboard on USRP N210 which samples at 4MHz.

LoRa transceiver. In the experiments, we test two LoRa transceivers, B-L072Z-LRWAN1 (SX1276, $860-930$MHz) and TTGO LoRa32 (SX1278, $433-470$MHz). The non-linear circuit is put between the evaluation boards and the antennas, as shown in Figure 12.

7 Evaluation

In this section, we evaluate the performance of LoRadar from three aspects: downlink transmission, uplink transmission and sensing accuracy.

7.1 Performance of Downlink Transmission

When evaluating downlink transmission, LoRa packets are embeded in the sensing signals, where each packet contains 1-byte payload. For each position, we log at least 1000 packets. We set BER that see no error to be 10^{-5}.

7.1.1 Transmission Range

We first evaluate the downlink transmission range of LoRadar in line-of-sight scenario. We do this set of experiment at the corridor outside the laboratory. The center frequency of the chirp is 900MHz. It sweeps 866MHz in 1ms. The receiver, SX1278, is configured to work at 433MHz, with a spreading factor of 7, 125kHz channel bandwidth and a code rate of $4/8$. The corresponding data rate is 3.4 kbps. We plot the RSSI values with respect to the transmission distance in Figure 13. As expected, we can find that RSSI values decrease as the receiver moves away from the LoRadar device. The RSSI values have some variations as there could be people walking on the corridor, blocking the light-of-sight. When the distance is beyond 16m (RSSI=-118dBm), bit error rate starts to increase, becoming larger than 1%.

We note that the transmission range of LoRadar is much shorter than the standard LoRa transceiver. This is because the harmonic is much weaker than the original signal. The sensitivity of LoRa nodes can be up to -148 dBm, which is about 30 dB lower than -118 dBm. In order to fully explore the good sensitivity of LoRa, we can extend the communication range by configuring the LoRa node to work at a lower data rate, as lower data rates require lower SNRs. Besides, in order to compensate for the power loss, we can also add an amplifier to amplify the desired harmonic. We leave this for future work.

7.1.2 Performance under NLoS Scenarios

We evaluate LoRadar's performance in non-light-of-sight (NLoS) scenarios. We put the LoRa receiver at four different locations: 1) in a paper box 2) behind a wooden door 3) behind a concrete wall and 4) in a handbag. The distance between the transmitter and receiver is fixed at 3m. Figure 14 shows the performance under different scenarios. As we can see, the performance is worst when the receiver is behind the concrete wall, as the wall can greatly attenuate the signal. It is a little unexpected that LoRadar shows the second highest BER when the receiver is in a handbag. By observing the phenomenon, we infer that the underlying reason is the misalignment between the TX and RX antenna. As we know, each antenna has a radiation pattern, i.e., polarization. Alignment of the polarization of TX and RX antennas will improve the signal quality. When we put the receiver inside a handbag, we are unable to control the orientation of the receiver's antenna. Thus, the polarization of the receiver's antenna is not aligned with the transmitter's, which lead to the high BER.

7.1.3 Impact of FMCW Chirp Bandwidth

We conduct this set of experiment to see whether the downlink performance is affected by the bandwidth of sensing signals. As LoRadar requires that $BW = 2f_L$, when we change BW, say from 200MHz to 1GHz, there may not have LoRa receivers working at the corresponding frequency (f_L should be from 100MHz to 500MHz). To conduct this experiment, we use the way shown in Figure 4 to generate the desired harmonic. The signal on the first TX antenna sweeps from f_1 to $f_1 + BW$ while the other antenna sweeps from f_2 to $f_2 + BW$ ($f_2 > f_1$). Signals are embeded into the second antenna. The LoRa receiver is configured to work at f_L, where $f_L = f_2 - f_1$ and we set f_1 to be 500MHz. We use two different LoRa receivers, working at 433MHz (SX1278), 868MHz and 915MHz (SX1276) respectively. The data rate is 3.4kbps.

Results are shown in Figure 15. When BW is 200MHz and 400MHz, there is no bit error. When BW continues

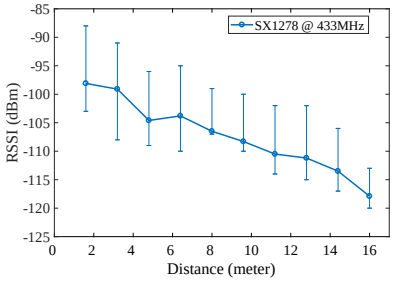

Fig. 13. RSSI vs distance.

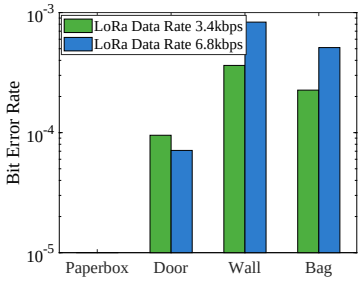

Fig. 14. Performance under NLoS.

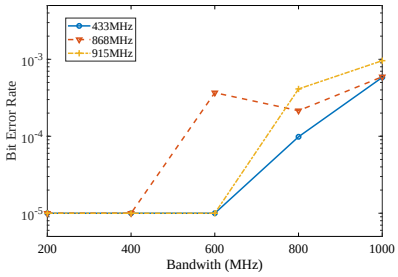

Fig. 15. Impact of FMCW chirp bandwidth.

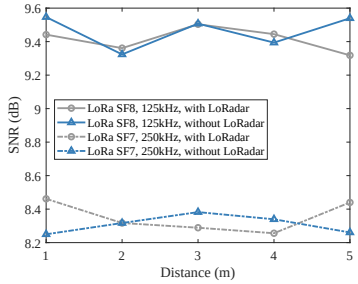

Fig. 16. There is no interference from LoRadar to other orthogonal LoRa links.

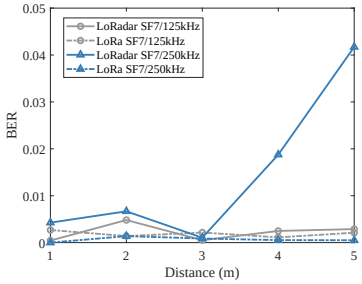

Fig. 17. Compare downlink performance of LoRadar and LoRa.

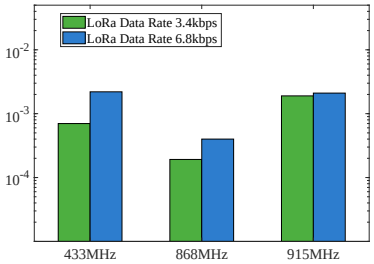

Fig. 18. Performance of working on SDR.

to increase, BERs also increase. We attribute these errors to the signal source. As we use a signal generator as the transmitter, the frequency sweeping waves are generated in the digital domain, where signals are discrete. This problem become obvious when the signal bandwidth is large, as the maximum sampling frequency is limited to 2.4GHz. Thus, the signals are actually not continuous waves. This should not be a problem on a radar, as voltage-controlled oscillators on the radar will generate analog signals, which are continuous.

7.1.4 Interference of LoRadar to other LoRa nodes

In this subsection, we evaluate the interference of LoRadar to other LoRa nodes. We compare the LoRa performance when there is a/no LoRadar device working nearby. A LoRadar Tx and a LoRa Tx are standing side by side, and they are communicating with their receivers (RX1 and RX2, also side by side), respectively.

In LoRa communication, signals are orthogonal when the spreading factor or the bandwidth is different. In other words, two LoRa links can be concurrent when either their spreading factor or bandwidth is different. Thus, to evaluate the interference of LoRadar on other LoRa links, we use orthogonal parameters for these two links. We set the spreading factor (SF) and bandwidth (BW) of LoRadar to be 7 and 125kHz. The other link employs two sets of parameters in turn: (SF=8, BW=125kHz) and (SF=7, BW=250kHz). The two links are working on the same (LoRa) band. We vary the distance between the transmitter and receiver, and evaluate the performance of the second link with the presence and absence of the first link.

We compare the SNR of the LoRa link in Figure 16. We can see that, there is no significant difference in SNR with/without LoRadar. It indicates that LoRadar will not cause significant interference to other nearby LoRa nodes. This is reasonable for two reasons. First, LoRa is designed to support concurrent transmission when the spreading factor or bandwidth is different. Second, LoRadar is not transmitting on the LoRa band. It is transmitting on the radar band. Thus, the signals from LoRadar will not interfere the other orthogonal LoRa signals.

7.1.5 Compare LoRadar with original LoRa

In this section, we compare the downlink performance of LoRadar and original LoRa. We set the transmission power of LoRadar and LoRa transmitter both to be 0dBm. Results are shown in Figure 17. We can see that, for SF7/125kHz, the performance of LoRadar and LoRa is close. For SF7/250kHz, the BER of LoRadar increases dramatically with growing distance. The possible reason is that, the non-linear harmonic is much weaker than the original signal, and when the distance increases, the SNR drops so that the channel capacity is insufficient to support the high data rate. It indicates that LoRadar is more suitable for low data rate applications, such as connecting low-rate, low-power sensors/actuators.

7.1.6 Performance of LoRadar on SDR

As the bandwidth of the USRP SDR is limited to 120MHz, we adopt the way in Section 7.1.3 to generate 100MHz frequency sweeping wave. One channel sweeps from 2GHz to 2.1GHz while the second channel sweeps from 2GHz+f_L to 2.1GHz+f_L. Similarly, we test LoRa receivers working at 433MHz (SX1278), 868MHz and 915MHz bands. To prevent the non-linear harmonic generated by the USRP circut, we use high pass filters to filter out signals below 1.2GHz.

Results are shown in Figure 18. BERs are higher compared with the results obtained using the signal generator (Figure 15). We also attribute the reason to the signal source. Similar to the signal generator, the frequency sweeping waves are generated in the digital domain. The frequency sweeping wave is of 100MHz bandwidth while the maximum sampling rate is 240MHz. The frequency of the signal is not changing in a continuous way. However, the results indicate the feasibility of deploying LoRadar on SDR devices. In the future when there are wide-band daughterboard for USRPs, LoRadar can be implemented on these devices.

7.2 Performance of Uplink

7.2.1 Transmission Range

We evaluate the communication distance of uplink transmission. The experiment is also conducted at the corridor outside the laboratory area. The LoRa transceiver is SX1278. It is configured to work at 433MHz and the data rate is 3.4kbps. We test three TX power levels: 5dBm, 11dBm and 17dBm. The LoRadar device generates linear chirps sweeping 864MHz in 0.5ms. Thus, the LoRa signals will be down-converted to baseband at 1MHz.

We plot BERs verus distance in Figure 19. There is no bit error within 20m when LoRa transmits with 11dBm or above power. When LoRa node is transmitting at 5dBm power level, BER becomes above 0.1% when the distance is 29m. Compared with downlink, the uplink transmission can achieve longer distance. This is because in the downlink, LoRa signals is the harmonic generated by the non-linear circuit, whose signal strength is weaker than the original signal. In order to achieve symmetric uplink and downlink communication distance, we could use a lower data rate for the downlink transmission.

7.2.2 Impact of FMCW Ramp Rate

In this experiment, we evaluate the impact of FMCW ramp rate on data transmission. The LoRadar device generates two 864MHz frequency sweeping waves, offset by half the chirp duration as shown in Figure 7. We test with five different chirp durations: 0.1ms, 1ms, 5ms, 10ms and 15ms. We also vary the LoRa data rates, using a spread factor of 7, coding rate of $4/8$, and bandwidth of 125kHz, 250kHz and 500kHz, respectively. From Figure 20, we can see that there is no obvious trend associated with BER and chirp duration. It indicates that, changing the FMCW ramp rate will not have impact on LoRa transmission. In other words, mixing signals on the two TX chains can create a stable carrier wave, regardless of the ramp rate of chirp signals. So, we can set the radar ramp rate and LoRa data rate independently, according to the sensing scenario and communication demand.

7.2.3 Concurrent LoRa Transmissions

In this experiment, we test LoRadar's performance on decoding concurrent LoRa transmissions. We deploy two LoRa nodes 3m away from the LoRadar device, both transmitting packets at 433MHz. One use spread factor 8, while the other use spread factor 9. We test with different LoRa data rates by using different channel bandwidths, *i.e.*, 125kHz, 250kHz and 500kHz.

Results are shown in Figure 21. We can see that LoRadar can decode concurrent orthogonal transmissions. There is no bit error for the one with lower data rate (spread factor 9); for the one with higher data rate (spread factor 8), BERs are below 0.05%. When the data rate of each node increases, the total channel goodput also increases.

7.3 Sensing Capability

In this section, we evaluate the sensing performance of LoRadar. According to previous research [3], the sensing capability of FMCW radar mainly stems from its ability to obtain two parameters, the frequency offset Δf and phase τ. The frequency offset is used to estimate the distance from the object to the radar while phase information can track the relative movement of the object. Other information, such as velocity, can be derived from these two parameters. Thus, we conduct this experiment to see whether LoRadar preserves the capability to estimate Δf and τ.

We first evaluate Δf estimation. The LoRadar device is doing downlink transmission using the waveform designed in Section 4. We put a laptop at different distances before the radar. We compare the estimated Δf with the one obtained using the orignal linear chirp. Results are shown in Figure 22. Each result is averaged over 5 measurements. As the linear chirp sweeps 866MHz band, the ranging resolution is 17cm. When $d = 50$cm, there is some ambiguity. Using both waveforms, Δf in four out of the five measurements gives 40kHz and the remaining one gives 42kHz. So the average is 40.4kHz. At all locations, both waveforms give the same Δf.

We then evaluate τ estimation. We put the same laptop on a camera slider. We control the slider by a remote controller to move the laptop back and forth before the LoRadar device. We compare the phase change of such a back-and-forth movement obtained using the modified waveform and the original waveform. Results are shown in Figure 23. We can see that, the phase change obtained using the designed waveform is highly correlated with the one obtained using the original waveform. The minimum displacement we tested is 1 inch, as it is the minimum displacement we can control using the slider.

From these results, we can conclude that, the modified waveform still preserves the sensing capability of a linear chirp. Embedding data signals into the waveform does not degrade its sensing resolution.

8 Related Work

Radio frequency as a sensing medium. Recent years have witnessed a surge of interest in using radio waves as the sensing media. These works mainly fall between two categories, using the commodity communication infrastructure (*i.e.*, Wi-Fi AP) or using the customized RF radar device. Along the first category, Wi-Fi sensing has shown promising results in many applications, such as gesture/activity recognition [14], [15], [16], [17], [18], vital sign monitoring [9], [19], [20] and imaging [21], [22]. The main challenges for Wi-Fi sensing include tracking multiple people simultaneously,

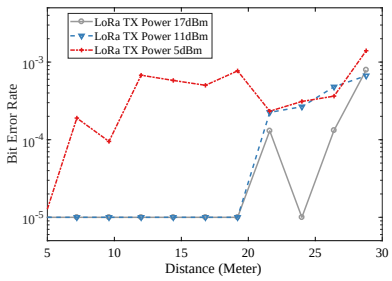

Fig. 19. Transmission Range.

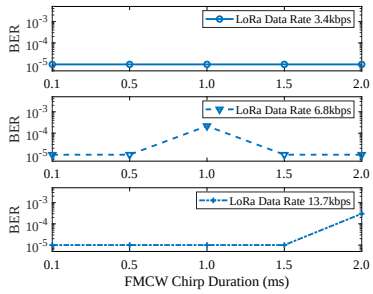

Fig. 20. Impact of FMCW chirp duration.

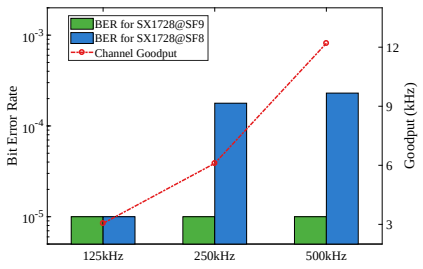

Fig. 21. Decoding concurrent transmissions.

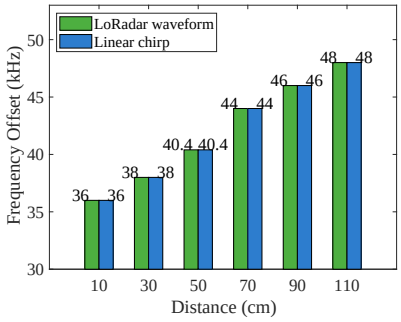

Fig. 22. Frequency offset estimation.

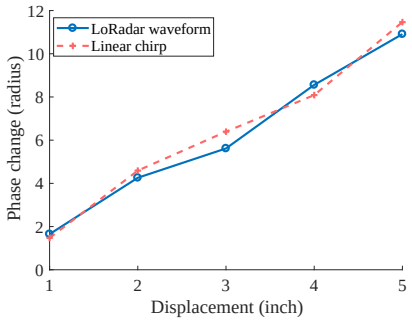

Fig. 23. Phase estimation.

adapting to new environments, limited resolution, etc. [23], [24].

As for the second category, both industry and academia are designing miniature Radar for home applications. Soli [2], the mmWave radar designed by Google, is able to recognize ubiquitous hand gestures. Researchers are also devoted to designing miniature Radar for monitoring breathing rate and heart rate [3], [4], gait velocity/stride length [25], and sleep stages [26], [27]. As radar signals are customized for sensing purpose, compared with Wi-Fi signals, it can achieve fine sensing granularity and can track multiple, concurrent moving body parts.

Joint radar-communication design. As there are unprecedented data traffic in both cellular and WLAN, spectrum sharing between radar and communication system has become an important research area [28], [29]. As the radar and communication systems may interfere with each other, in order to address their coexistence issue, there is on-going research on joint radar-communication design [30]. Existing works address this problem from different aspects. Some works discuss how to mitigate the interference between the communication system and radar system [31] while others design dual-function waveforms [32], [33], which can be used both for sensing and communication. LoRadar belongs to the second category. Different from existing work, LoRadar does not require a dedicated receiver to decode the customized waveforms and can talk directly with LoRa nodes.

Non-linearity. Traditionally regarded as harmful, non-linear effect has been exploited to enable many interesting applications. BackDoor [34] enables smartphones to record ultrasound utilizing non-linearity in acoustic amplifiers. With the same observation, Lin *et al.* [35] built an ultrasonic indoor localization system on smartphones. Vasisht *et al.* [7] took advantage of non-linearity to mitigate interference for in-body backscatter. In [6], An *et al.* enabled cross-frequency communication by exploiting the non-linearity of RFID tags. E-eyes [36] takes the nonlinear response from electronic circuits as the fingerprint to identify hidden electronic devices.

9 Discussion

In this section, we discuss some remaining issues in this paper.

LoRadar implementation on a miniature radar. Due to the limited API of commercial miniature radars on the market, in this paper, we use a signal generator to transmit the designed waveforms, which is a piecewise function where each piece is a linear chirp.

Here we discuss how to implement LoRadar on a miniature radar. For the downlink part, LoRadar requires that the transmitter have at least two antennas. Current radars are usually designed to be a multi-antenna device so as to combat multi-path phenomenon and achieve good sensing performance [5], [10]. Commercial radar usually employs a chirp engine to generate the frequency sweeping waves [13]. The chirp engine is a Fractional-N phase locked loops (PLL) frequency synthesizer, which can achieve sub-Hz frequency resolution [37]. In addition, the chirp duration and sweeping bandwidth are both programmable parameters. Thus, we can program the chirp engine to generate the designed waveform in Section 4. For the uplink part, compared with the normal FMCW radar, the receiving chain of LoRadar is also slightly different. As shown in Figure 10, in addition to down-converting the sensing signals, LoRadar also needs to down-convert the data signals. Thus, LoRadar requires

extra mixers and combiners. Combining downlink and uplink design, LoRadar requires some hardware modification which will not increase the cost substantially.

MAC layer design. As the channel access mechanism of LoRa defined in LoRaWAN is aloha in nature, LoRadar can fully support the MAC layer operations. LoRaWAN defines three classes of nodes, Class A, Class B and Class C. To be specific, for Class A and C, downlink transmission is initiated by an uplink transmission. So the LoRadar device can stay in RX state and listen for uplink transmission. Downlink transmission can be carried out in the corresponding RX windows following the uplink transmission. For class B, the LoRadar device can send beacons periodically as the gateway. When there is downlink data to a specific node, the LoRadar device can carry out downlink transmission in the corresponding slot; for the remaining time, it can stay in the RX state, listening for uplink transmission. Therefore, with the downlink and uplink design present in this paper, LoRadar can support the MAC layer protocol of LoRaWAN.

Joint radar-communication paradigm. Compared with directly adding a LoRa radio to the radar, joint radar-communication paradigm has its unique advantage in a smart home scenario. First, it improves the spectrum efficiency by reusing the spectrum for both sensing and data communication; second, it addresses the coexistence issue between radar system and communication system; third, as there are many possibilities to design the radar signals, it is our future work to enable LoRadar to communicate with other IoT devices, such as Bluetooth or Zigbee devices. Thus, we envision that the radar can become the central control unit in a smart home that is able to connect with and coordinate various types of IoT devices.

10 Conclusion

In this paper, we present LoRadar, a joint radar-communication paradigm where the radar can communicate with LoRa devices while performing sensing tasks. LoRadar converts wideband sensing signals into a narrowband signal by exploiting the non-linearity effect of RF circuits. For downlink transmission, we design the dual-function radar signals so that its sensing capability is preserved while the non-linear harmonic is a standard LoRa signal. For uplink transmission, we present a new receiving chain design that is capable of both radar sensing and data decoding. We implement and evaluate LoRadar from various aspects. Evaluation results show that LoRadar can achieve home-level coverage range with 3.4kbps data rate while it preserves the sensing resolution of the radar.

Acknowledgement

This work is partially supported by the RGC under Contract CERG 16204418, 16203719, R8015, the National Natural Science Foundation of China (No. 62002150), the Guangdong Key Research and Development Program (No. 2019B121204009), the Guangdong Natural Science Foundation (No. 2017A030312008) and the project of "FANet: PCL Future Greater-Bay Area Network Facilities for Large-scale Experiments and Applications (No. LZC0019)".

References

[1] M. Zhao, T. Li, M. Abu Alsheikh, Y. Tian, H. Zhao, A. Torralba, and D. Katabi, "Through-wall human pose estimation using radio signals," in *Proceedings of the IEEE Conference on Computer Vision and Pattern Recognition*, 2018, pp. 7356–7365.

[2] J. Lien, N. Gillian, M. E. Karagozler, P. Amihood, C. Schwesig, E. Olson, H. Raja, and I. Poupyrev, "Soli: Ubiquitous gesture sensing with millimeter wave radar," *ACM Transactions on Graphics (TOG)*, vol. 35, no. 4, p. 142, 2016.

[3] F. Adib, H. Mao, Z. Kabelac, D. Katabi, and R. C. Miller, "Smart homes that monitor breathing and heart rate," in *Proceedings of the 33rd annual ACM conference on human factors in computing systems*. ACM, 2015, pp. 837–846.

[4] S. Yue, H. He, H. Wang, H. Rahul, and D. Katabi, "Extracting multi-person respiration from entangled rf signals," *Proceedings of the ACM on Interactive, Mobile, Wearable and Ubiquitous Technologies*, vol. 2, no. 2, p. 86, 2018.

[5] M. Zhao, Y. Tian, H. Zhao, M. A. Alsheikh, T. Li, R. Hristov, Z. Kabelac, D. Katabi, and A. Torralba, "Rf-based 3d skeletons," in *Proceedings of the 2018 Conference of the ACM Special Interest Group on Data Communication*. ACM, 2018, pp. 267–281.

[6] Z. An, Q. Lin, and L. Yang, "Cross-frequency communication: Near-field identification of uhf rfids with wifi!" in *Proceedings of the 24th Annual International Conference on Mobile Computing and Networking*. ACM, 2018, pp. 623–638.

[7] D. Vasisht, G. Zhang, O. Abari, H.-M. Lu, J. Flanz, and D. Katabi, "In-body backscatter communication and localization," in *Proceedings of the 2018 Conference of the ACM Special Interest Group on Data Communication*. ACM, 2018, pp. 132–146.

[8] "Smart homes & buildings," https://www.semtech.com/lora/lora-applications/smart-homes-buildings.

[9] Y. Zeng, D. Wu, R. Gao, T. Gu, and D. Zhang, "Fullbreathe: Full human respiration detection exploiting complementarity of csi phase and amplitude of wifi signals," *Proceedings of the ACM on Interactive, Mobile, Wearable and Ubiquitous Technologies*, vol. 2, no. 3, p. 148, 2018.

[10] F. Adib, Z. Kabelac, and D. Katabi, "Multi-person localization via {RF} body reflections," in *12th {USENIX} Symposium on Networked Systems Design and Implementation ({NSDI} 15)*, 2015, pp. 279–292.

[11] "Sms7630 series," http://www.skyworksinc.com/Product/511/SMS7630_Series.

[12] G. A. Vera, Y. Duroc, and S. Tedjini, "Third harmonic exploitation in passive uhf rfid," *IEEE Transactions on Microwave Theory and Techniques*, vol. 63, no. 9, pp. 2991–3004, 2015.

[13] "Ti mmwave sensor," http://www.ti.com/product/IWR1443.

[14] L. Sun, S. Sen, D. Koutsonikolas, and K.-H. Kim, "Widraw: Enabling hands-free drawing in the air on commodity wifi devices," in *Proceedings of the 21st Annual International Conference on Mobile Computing and Networking*. ACM, 2015, pp. 77–89.

[15] A. Virmani and M. Shahzad, "Position and orientation agnostic gesture recognition using wifi," in *Proceedings of the 15th Annual International Conference on Mobile Systems, Applications, and Services*. ACM, 2017, pp. 252–264.

[16] Y. Ma, G. Zhou, S. Wang, H. Zhao, and W. Jung, "Signfi: Sign language recognition using wifi," *Proceedings of the ACM on Interactive, Mobile, Wearable and Ubiquitous Technologies*, vol. 2, no. 1, p. 23, 2018.

[17] R. H. Venkatnarayan, G. Page, and M. Shahzad, "Multi-user gesture recognition using wifi," in *Proceedings of the 16th Annual International Conference on Mobile Systems, Applications, and Services*. ACM, 2018, pp. 401–413.

[18] W. Jiang, C. Miao, F. Ma, S. Yao, Y. Wang, Y. Yuan, H. Xue, C. Song, X. Ma, D. Koutsonikolas *et al.*, "Towards environment independent device free human activity recognition," in *Proceedings of the 24th Annual International Conference on Mobile Computing and Networking*. ACM, 2018, pp. 289–304.

[19] H. Wang, D. Zhang, J. Ma, Y. Wang, Y. Wang, D. Wu, T. Gu, and B. Xie, "Human respiration detection with commodity wifi devices: do user location and body orientation matter?" in *Proceedings of the 2016 ACM International Joint Conference on Pervasive and Ubiquitous Computing*. ACM, 2016, pp. 25–36.

[20] H. Abdelnasser, K. A. Harras, and M. Youssef, "Ubibreathe: A ubiquitous non-invasive wifi-based breathing estimator," in *Proceedings of the 16th ACM International Symposium on Mobile Ad Hoc Networking and Computing*. ACM, 2015, pp. 277–286.

[21] D. Huang, R. Nandakumar, and S. Gollakota, "Feasibility and limits of wi-fi imaging," in *Proceedings of the 12th ACM Conference on Embedded Network Sensor Systems*. ACM, 2014, pp. 266–279.
[22] C. R. Karanam and Y. Mostofi, "3d through-wall imaging with unmanned aerial vehicles using wifi," in *2017 16th ACM/IEEE International Conference on Information Processing in Sensor Networks (IPSN)*. IEEE, 2017, pp. 131–142.
[23] H. Jiang, C. Cai, X. Ma, Y. Yang, and J. Liu, "Smart home based on wifi sensing: A survey," *IEEE Access*, vol. 6, pp. 13 317–13 325, 2018.
[24] Y. Ma, G. Zhou, and S. Wang, "Wifi sensing with channel state information: A survey," *ACM Computing Surveys (CSUR)*, vol. 52, no. 3, p. 46, 2019.
[25] C.-Y. Hsu, Y. Liu, Z. Kabelac, R. Hristov, D. Katabi, and C. Liu, "Extracting gait velocity and stride length from surrounding radio signals," in *Proceedings of the 2017 CHI Conference on Human Factors in Computing Systems*. ACM, 2017, pp. 2116–2126.
[26] C.-Y. Hsu, A. Ahuja, S. Yue, R. Hristov, Z. Kabelac, and D. Katabi, "Zero-effort in-home sleep and insomnia monitoring using radio signals," *Proceedings of the ACM on Interactive, Mobile, Wearable and Ubiquitous Technologies*, vol. 1, no. 3, p. 59, 2017.
[27] M. Zhao, S. Yue, D. Katabi, T. S. Jaakkola, and M. T. Bianchi, "Learning sleep stages from radio signals: A conditional adversarial architecture," in *Proceedings of the 34th International Conference on Machine Learning-Volume 70*. JMLR. org, 2017, pp. 4100–4109.
[28] A. D. Singh, S. Vishwakarma, and S. S. Ram, "Co-channel interference between wifi and through-wall micro-doppler radar," in *2017 IEEE Radar Conference (RadarConf)*. IEEE, 2017, pp. 1297–1302.
[29] H.-A. Safavi-Naeini, S. Roy, and S. Ashrafi, "Spectrum sharing of radar and wi-fi networks: The sensing/throughput tradeoff," *IEEE Transactions on Cognitive Communications and Networking*, vol. 1, no. 4, pp. 372–382, 2015.
[30] B. Paul, A. R. Chiriyath, and D. W. Bliss, "Survey of rf communications and sensing convergence research," *IEEE Access*, vol. 5, pp. 252–270, 2017.
[31] L. Zheng, M. Lops, X. Wang, and E. Grossi, "Joint design of overlaid communication systems and pulsed radars," *IEEE Transactions on Signal Processing*, vol. 66, no. 1, pp. 139–154, 2018.
[32] F. Liu, L. Zhou, C. Masouros, A. Li, W. Luo, and A. Petropulu, "Toward dual-functional radar-communication systems: Optimal waveform design," *IEEE Transactions on Signal Processing*, vol. 66, no. 16, pp. 4264–4279, 2018.
[33] C. Sahin, J. Jakabosky, P. M. McCormick, J. G. Metcalf, and S. D. Blunt, "A novel approach for embedding communication symbols into physical radar waveforms," in *2017 IEEE Radar Conference (RadarConf)*. IEEE, 2017, pp. 1498–1503.
[34] N. Roy, H. Hassanieh, and R. Roy Choudhury, "Backdoor: Making microphones hear inaudible sounds," in *Proceedings of the 15th Annual International Conference on Mobile Systems, Applications, and Services*. ACM, 2017, pp. 2–14.
[35] Q. Lin, Z. An, and L. Yang, "Rebooting ultrasonic positioning systems for ultrasound-incapable smart devices," *arXiv preprint arXiv:1812.02349*, 2018.
[36] Z. Li, Z. Yang, C. Song, C. Li, Z. Peng, and W. Xu, "E-eye: Hidden electronics recognition through mmwave nonlinear effects," in *Proceedings of the 16th ACM Conference on Embedded Networked Sensor Systems*. ACM, 2018, pp. 68–81.
[37] "Adf4158," https://www.analog.com/en/products/adf4158.html#product-overview.

Qianyi Huang is a research assistant professor from Southern University of Science and Technology, Shenzhen, China. She received her Ph.D. degree in Department of Computer Science and Engineering from Hong Kong University of Science and Technology and her bachelor's degree in Computer Science from Shanghai Jiao Tong University. Her research interests lie in mobile computing, Internet-of-Things and security.

Zhiqing Luo is currently pursuing his Ph.D degree at School of Electronics and Information Engineering, Huazhong University of Science and Technology, Hubei, China. Before that, he has received his Bachelor Degree in Communication Engineering from Jilin University, Jilin, China, in June 2016. His research interests include PHY/MAC designs and IoT security in wireless networks.

Jin Zhang (S'06-M'09-) is currently an assistant professor in Computer Science and Engineering Department, Southern University of Science and Technology, Shenzhen, China. She graduated from Department of Electronic Engineering at Tsinghua University in 2004 with a bachelor's degree and in 2006 with a master's degree. She received the Ph.D. degree from Department of Computer Science and Engineering, Hong Kong University of Science and Technology. Her research interests are mainly in next-generation wireless networks, network economics, mobile computing in healthcare, cooperative communication and networks.

Wei Wang (S'10-M'16-SM'20) is currently a full professor with the School of Electronic Information and Communications, Huazhong University of Science and Technology. He received the Ph.D. degree from the Department of Computer Science and Engineering, The Hong Kong University of Science and Technology. His research interests include PHY/MAC design and mobile computing in wireless systems. He has published 2 books and 70 refereed papers in international leading journals and primer conferences. He is the inventor of 3 US and 20 Chinese patents. He won the best paper award in IEEE ICC 2019. He was selected as Young Elite Scientist Sponsorship Program, China Association for Science and Technology, and Hundred Talents Program, Hubei Province, China. He served on TPC of INFOCOM, GBLOBECOM, ICC, etc. He served as Editors for IEEE Access, IJCS, China Communications, and Guest Editors for Wireless Communications and Mobile Computing and the IEEE COMSOC MMTC COMMUNICATIONS.

Qian Zhang (M'00-SM'04-F'12) joined Hong Kong University of Science and Technology in Sept. 2005 where she is a full Professor in the Department of Computer Science and Engineering. Before that, she was in Microsoft Research Asia, Beijing, from July 1999, where she was the research manager of the Wireless and Networking Group. Dr. Zhang has published about 300 refereed papers in international leading journals and key conferences in the areas of wireless/Internet multimedia networking, wireless communications and networking, wireless sensor networks, and overlay networking. She is a Fellow of IEEE for "contribution to the mobility and spectrum management of wireless networks and mobile communications". Dr. Zhang has received MIT TR100 (MIT Technology Review) worlds top young innovator award. She also received the Best Asia Pacific (AP) Young Researcher Award elected by IEEE Communication Society in year 2004. Dr. Zhang received the B.S., M.S., and Ph.D. degrees from Wuhan University, China, in 1994, 1996, and 1999, respectively, all in computer science.